Journal of Applied Fluid Mechanics, Vol. 16, No. 12, pp. 2569-2580, 2023.
Available online at www.jafmonline.net, ISSN 1735-3572, EISSN 1735-3645.
https://doi.org/10.47176/jafm.16.12.1694

Aerodynamic Improvements of Buses Inspired by Beluga Whales

S. K. Arabaci and M. Pakdemirli†

Department of Mechanical Engineering, Manisa Celal Bayar University, Muradiye, Yunusemre, Turkey

†*Corresponding Author Email: pakdemirli@gmail.com*

ABSTRACT

The innovative bus designs, inspired by the whales, have been developed. The designs are confined to the frontal area of the buses. The new designs are named as the Beluga buses. Several variants of the models all mimicking Beluga whales are proposed. Both numerical analysis and experimental have been conducted to determine the drag coefficients of various models. The ANSYS CFD program was used for numerical simulations. WT tests were conducted to experimentally determine the drag coefficients. Both methods indicate that the beluga-inspired buses offer significant reductions in drag, which can lead to lower fuel consumption. The new beluga design is expected to reduce fuel consumption by 12.64%. Comparing the experimental and numerical results, a 6.4% discrepancy in the drag coefficients is observed at low Reynolds numbers, which became negligible at higher Reynolds numbers. The new geometry is expected to offer an economical solution for reducing fuel consumption.

Article History

Received December 4, 2022
Revised July 31, 2023
Accepted July 31, 2023
Available online October 8, 2023

Keywords:

Aerodynamics
Biomimetics
Drag Coefficients
CFD
WT Tests
Buses

1. INTRODUCTION

Biomimetics refers to the field of science that involves the development of technology by imitating nature's forms and structures. The designs of living organisms serve as the primary source of inspiration for creating more efficient and effective designs (Benyus, 2002). Biomimetics has wide-ranging applications, from robotics and nanotechnology, to aviation, materials science, aerospace and architecture.

The complexity and perfection of natural designs often require extensive computations to reveal. Computational fluid dynamics (CFD) has proven to be an efficient tool for studying biomimetics (Yan, 2007). Biomimicry involves imitating natural forms to create innovative designs that exhibit improved fluid-structure interactions. When designing for objects immersed in fluid, such as a body, the objective is often to minimize drag, maximize lift, bolster stability, and optimize maneuverability. Researchers have discovered that the structure of humpback whale fins, which possess tubercles, can effectively reduce drag. Biomimetic bumps are used in aircraft and turbine designs. (https://seas.harward.edu) Usage of tubercles on the wings could improve and reduce fuel cost (Fish et al., 2011). 16% of the total energy exhaust in US is attributed to aerodynamic drag, making reduction of drag a crucial component in achieving energy savings. Scientists are actively working to modify the shape and weight of vehicles in order to achieve lower drag coefficients. Research has shown that aerodynamic improvement is a critical technology for fuel reduction in vehicles. Mercedes-Benz has designed a bionic car, inspired by the shape of a boxfish, that achieved a low drag coefficient of 0.19, compared to the typical range of 0.30-0.35 for car models. By modifying the truck, solving with k-ε model can result in estimated fuel savings of nearly 35% (Roy & Srinavasan 2000). In the case of buses, reducing aerodynamic drag up to 14% through slight modifications in the shape can result in an 8.4% reduction in fuel consumption (Mohamed et al., 2015). Using a curved surface in front can reduce the drag coefficient from 0.8782 to 0.3872 in another bus model (Bhave & Taherian 2014). Modifying the rear of buses has also been shown to substantially reduce total drag (Patil et al., 2012, Alamaan et al., 2014).

CFD method for predicting the drag coefficient is comparable to the WT tests with an accuracy of up to 4% (Ahmad et al., 2010). WT tests performed on a typical tractor and trailer configuration revealed that mirrors contribute to approximately 2% of the total drag (Belzile et al., 2012). Another study examined the impact of different diffuser angles on the aerodynamic of a simplified sedan. It was found that increasing the diffuser angle initially reduced, then increased the total aerodynamic drag coefficient, while decreasing the total aerodynamic lift coefficient. The introduction of a rear wind-break to the sedan resulted in a 1.7% reduction in drag (Hu & Wang 2011). A study on sports utility vehicles showed that add-on devices can reduce the aerodynamic

Nomenclature

C_d	drag coefficient	μ	fluid dynamics viscosity
C_f	skin friction	τ_ω	wall shear stress
F_d	drag force	**Acronyms**	
Re	Reynolds number	CFD	Computational Fluid Dynamics
U^*	friction velocity	PISO	Pressure Implicit of Split Operations
Units		UG	Unigraphics
m	meter	RANS	Reynolds Averaged Navier-Stokes
s	second	WT	Wind Tunnel
ρ	fluid density		

drag coefficient by 8% (Singha et al., 2014). A study conducted by Sudin et al. (2014) evaluated the impact of active and passive flow control methods on drag coefficients of vehicles. On a related note, the design of the A300-600ST cargo plane, also known as the Airbus Beluga, drew inspiration from the streamlined bodies and high volumetric shape of beluga whales (www.airbus.com). The Beluga is considered one of the world's most remarkable airplanes. All of the studies mentioned above focused on reducing aerodynamic drag through variations in body shape, including the research conducted (Daimler, & Mercedes-Benz 2011; Airbus, 2015; Trinh et al., 2022; Yudianto et al., 2022) in this area.

In this study, the aim is to reduce the aerodynamic drag by designing new buses body inspired by the shapes of beluga whales. Different bus models are constructed based on the beluga geometry and it is shown that significant reductions in drag forces and coefficients can be achieved with these new nature-inspired designs. The new buses, inspired by the whale head, will improve fuel economy and reduce fuel consumption and carbon dioxide release to the air. This is important for achieving a low carbon economy and sustainable development.

2. COMPUTATIONAL METHODOLOGY

The equations are composed of potential flow for fluid dynamics, Euler equations, Boltzmann equations, and Navier Stokes equations. Computational simulation methods rely on the fundamental principles of fluid dynamics included in the Navier-Stokes equations. (Wood, 2015). In CFD simulation, a comparison is made between k-ε and k-ω to determine the best model to use in literature. The k-ε model, introduced by Jones and Launder, solves the equations for turbulence and energy dissipation rate for calculating local turbulent viscosity. The initial coefficients for the model are 1.55, 2.0, and 0.09 for C_1, C_2, and C_μ, respectively (Jones & Launder 1973). These values were later updated by Launder and Spalding (1974) to 1.44 and 1.92 for C_1 and C_2, respectively. k-ω is another two-equation turbulence model that performs better in adverse pressure gradients and addresses limitations of the k-ε model (Wilcox, 1988, 2006, 2008)

The Navier-Stokes equations play a crucial role in CFD as they describe the airflow over various objects. As a more practical alternative for engineering applications like ground vehicles, the Reynolds-averaged Navier-Stokes (RANS) approach is commonly used. The RANS equations average out the instantaneous turbulent fluctuations over time, resulting in a set of equations that describe the time-averaged flow properties. Turbulent flow exhibits a wide range of vortex sizes, making it challenging to simulate accurately. In the RANS approach, the instantaneous turbulent fluctuations at all scales are not directly resolved. Instead, RANS models provide a time-averaged representation of the entire turbulent flow field, while the effects of unresolved turbulence are approximated using turbulence closure models, such as turbulence kinetic energy (k) and its dissipation rate, or the k-ε or k-ω models.

In this study, we used the k-ω SST model. This model was chosen because it has been shown to produce results that are both accurate and comparable to those obtained from the k-ε model.

In fluid flow simulation, The PISO algorithm was employed to ensure the proper coupling between pressure and velocity fields. The pressure interpolation was executed to a second order accuracy, while the Green-Gauss node-based scheme was utilized for gradient interpolation. The momentum equations were discretized using bounded central differencing, and the turbulence model equations were discretized using a second-order method. Time discretization was executed with a second-order implicit approach. The commercial CFD Ansys Fluent software was employed to perform these simulations. The simulations used the second-order implicit approach for the momentum equation, turbulent kinetic energy equation, and specific dissipation rate equation. (Jasak, 1996; Ferziger et al., 1997).

3. DETERMINATION OF THE GEOMETRY

Our new model designs draw inspiration from the distinctive body shapes of beluga whales, which can reach lengths of 5.5 m and weigh up to 1600 kg. These aquatic mammals are capable of sustaining speeds of up to 22 km/h for up to 15 minutes, a remarkable accomplishment in the dense fluid medium they inhabit (Nowak 1991). Figure 1 portrays the shape of a beluga.

In this paper, the drag coefficients and forces of newly designed beluga-inspired bus models are compared to that of the Neoplan Skyliner. (Fig. 2), This design is renowned for its exceptionally low drag coefficient, making it one of the most aerodynamically efficient. The physical characteristics and drag coefficient value (0.41) for the Skyliner have been provided by MAN Truck & Bus AG. To visualize the Skyliner, an illustration has been created

Fig. 1 Beluga whale

Fig. 2 Neoplan Skyliner Bus (Neoplan, 2023)

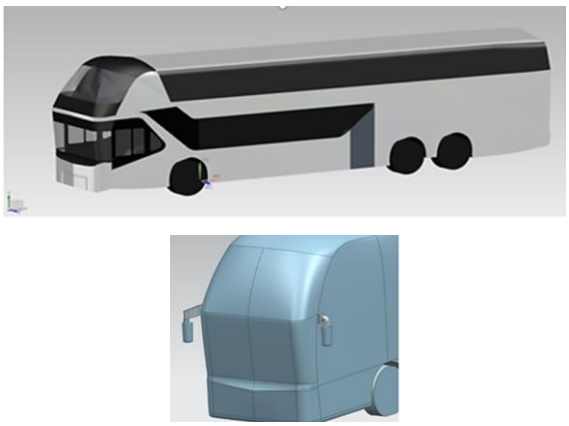

Fig. 3 3D model of the Skyliner (drawn in UG)

using the UG program, as depicted in Fig. 3. The Neoplan Skyliner has a length of 14 m, width of 2.55 m, and height of 4 m (https://www.neoplan.com).

Prior to the design of the new beluga buses, a comparable approach was employed to create a solid model of the beluga whale. Figure 4 provides a visualization of the process used to generate the 3D shape.

A set of six distinct models of beluga buses has been created and designated unique names, namely Bel.1.1, Bel.1.2, Bel.1.3, Bel.2.1, Bel.2.2, and Bel.2.3. Figure 5 provides an illustration of each model's shape. The first

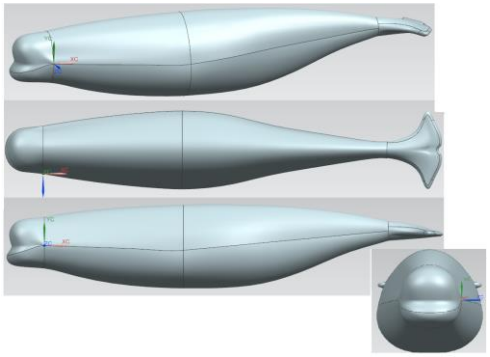

Fig. 4 Beluga whale 3D model

digit in the model name signifies the precise shape of the bus's frontal portion, while the second digit corresponds to the specific shape of the bus's middle and rear sections.

While the original bus model, drawn with the same dimensions, is defined as Sky.N, bus models that are compatible with whale designs and have the same volume as whale buses are known as Sky.V. To comply with highway regulations regarding bus dimensions, Beluga models with a reduced volumetric space of 100 m^3 have been selected instead of the original Neoplan Skyliner, named Sky.N, which has a volumetric space of 122.8 m^3. The characteristic length is taken as 13m.

To indicate models with a 1:40 reduction in dimensions that are used as test models in a WT, the suffix P is used, called as Sky.P.

The Sky.V with 100 m^3 volumetric space is a bus model designed to be compatible with whale designs, and it shares the same volume as other whale buses. New bus length is 13m.

The Beluga 2.x models have the same designed bodies as the Beluga 1.x models, but the front shape (nose) is somewhat different.

During the surface knitting process of all new designs, a 2.5 m extension is (shown in Fig. 6 as part B) deliberately left between the body and the head.

When inspecting the body components of the buses, it becomes apparent that the x.1 variants feature a design resembling that of a raindrop, whereas the x.2 models exhibit a widened middle section achieved by increasing the z-axis length by 0.25 m (Fig. 5). This dimension is shown in Fig. 6 as part A. On the other hand, the x.3 version maintains the same body shape as the Skyliner model. These distinctions are visible in Fig. 6, as depicted from the top view. Figure 5 provides the coordinate system and Bel.1.1 Bus Model.

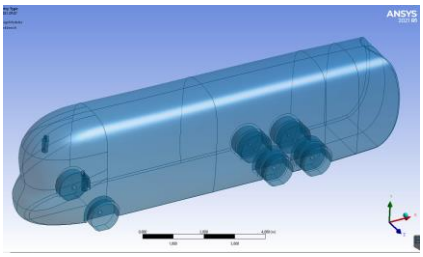

Fig. 5 Coordinate system and Bel.1.1 Bus model

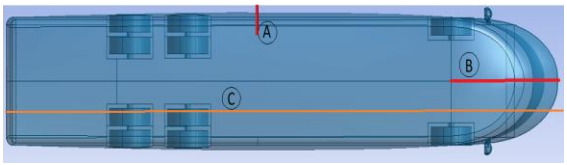

Fig. 6 Top view of the bus geometry

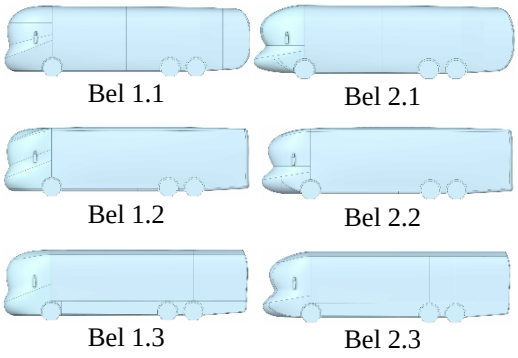

Fig. 7 Beluga buses (left side view)

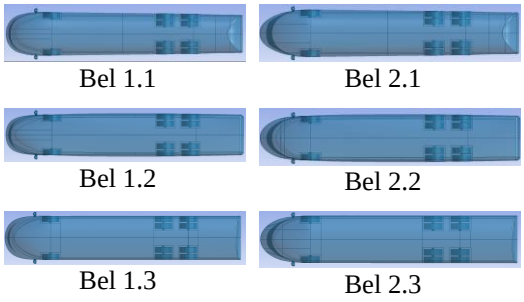

Fig. 8 Beluga buses (top view)

When the rear sides are examined, the x.1 models are curved, the x.2 model is bluntly drawn, the x.3 models are the same as the Skyliner rear form. These features of buses are seen in Fig. 7 and 8.

4. METHODS

To assess the aerodynamic performance of the new bus designs, both computational and experimental analyses are carried out.

4.1 Computational Methods

The ANSYS WORKBENCH software is employed to accurately position the models within a control volume measuring 22.5 meters in length, 12 meters in width, and 98 meters in height. The control volume is designed to be twice the length of the bus from the inlet, four length of the bus from the outlet, and eight width of the bus from the sides. The Sky.N model exhibits a blockage rate of 3.7%, while its dimensions are 2.55 m x 4 m x 14 m, resulting in a blockage ratio of 0.037. To ensure the validity of the findings, it is crucial to maintain a blockage ratio below 7.5%. The blockage ratio is calculated by dividing the cross-sectional area of the experimental model by the cross-sectional area of the WT test room. By adhering to this criterion, reliable and accurate results can be obtained.

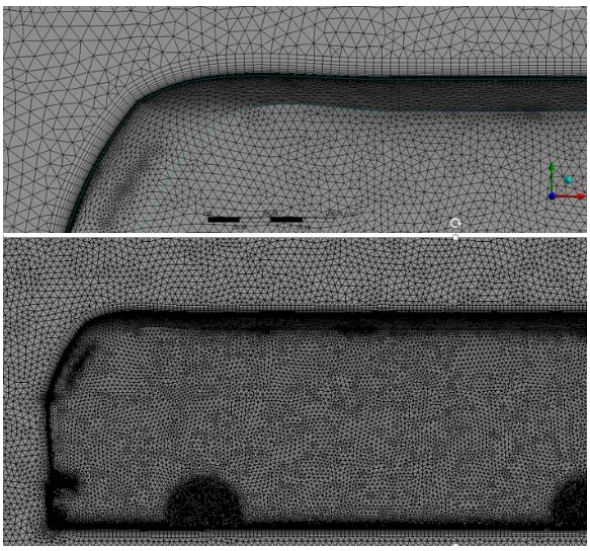

Fig. 9 Meshing of the Sky.N Model

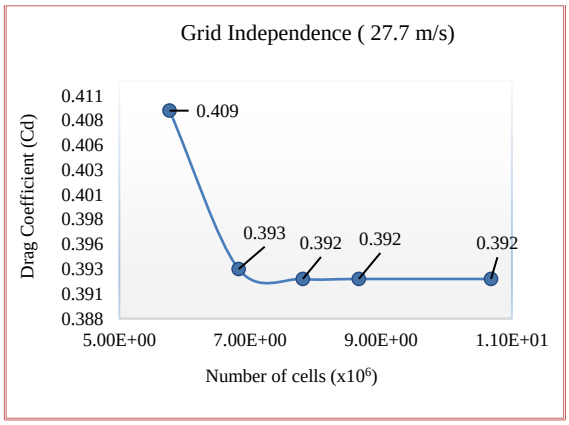

Fig. 10 Grid independence at 100 km/h

4.1.1 Grid Independence

The model is encompassed by rectangular prism-shaped enclosures, with a smaller mesh size employed within the inner box

Meshing of the Sky.N model is shown in Fig. 9. To test grid-independency regarding drag coefficient (Fig. 10), five different total cell numbers were employed. Results show that the 8,659,763 cell count yields ideal convergence.

4.1.2 Boundary Conditions

The simulations are conducted by applying specific boundary conditions, which consist of a velocity of 27.7 m/s at the inlet, at the outlet, pressure is taken equal to reference pressure which is 101325 Pa (1 atm). The road and bus surfaces are selected as a no-slip condition. On the other hand, a free-slip condition is applied at the sides of the models, allowing for fluid flow without any significant friction or resistance. The road is modeled as a moving surface, while the symmetry model is employed for computational fluid dynamics (CFD) analysis.

For comparison purposes with the experimental tests, however, the road is modeled in CFD as a non-moving road condition later in the analysis. The experimental data is compared with CFD for 1:40 scale buses. In the analysis, temperature, dynamic viscosity and air density

values are set to 15.5°C, 1.79 × 10^{-5} kg/ms and 1.225 kg/m³, respectively.

When conducting flow analysis using CFD, it is essential to consider the boundary layer thickness. During the pre-processing stage of CFD, it is necessary to determine the appropriate size for the first layer of grid cells in order to maintain the y+ (y-plus) value within the desired range. While the exact flow field is only known after solving the equations, it can be beneficial to make an initial prediction of the cell size to minimize the need for remeshing later on. In addition, including boundary layer computations in the analysis is crucial to achieve accurate results. The parameters are (Fluent, 2012)

$$C_f = 0.058\,\mathrm{Re}^{-0.2} \tag{1}$$

$$\tau_w = 0.5\rho C_f V^2 \tag{2}$$

$$U^* = \sqrt{\frac{\tau_w}{\rho}} \tag{3}$$

$$y = \frac{y^+ \mu}{U^* \rho} \tag{4}$$

The skin friction (C_f) is calculated using Eq. (1), and the wall shear stress (τ_w) is calculated using Eq. (2). The friction velocity (U^*) is calculated using Eq. (3).

One important significance in CFD simulations is the selection of suitable mesh configuration and turbulence model. A solution criterion that can guide this selection is the value of y^+, which is a dimensionless parameter that describes the treatment of the flow near a wall. Values of $y^+ \approx 1$ are preferred for near-wall modeling. This means that choosing an appropriate y^+ value can help ensure accurate and efficient simulations. By considering y^+ values in conjunction with other factors, such as the Reynolds number and the geometry of the system being simulated, researchers can improve the accuracy and reliability of CFD simulations.

In this study, the k-ω SST turbulence model is selected, which is widely suggested for simulating external flows. The distance of the first computational cell from the wall, denoted as y, is determined using Eq. (4) with the condition y+= 1. Here, y represents the thickness of the first layer in the computational fluid dynamics (CFD) analysis.

4.1.3 Calculating the Drag Force and the Drag Coefficient

The drag force is given in Eq (5);

$$F_d = 0.5\rho C_d A U^2 . \tag{5}$$

The models are compared using a fixed volume of 100 m³, except for Sky.N (122.8 m³). The varying cross-sectional areas of the models may cause slight differences. Drag force depends on fluid density (ρ), drag coefficient (C_d), cross-sectional area perpendicular to the airflow direction (A), and fluid velocity (U). The V model is to reduce the Skyliner body to a certain extent and define each body as equal and 100 m³. The V model is used to analyze a symmetrical model. When compared to experimental data, the analysis is repeated using the WT with adapted boundary conditions, and this new approach is named as the P model (such as Bel 1.2 P, Bel 2.2 P etc.)

Table 1 The parameters in WT experiments

Models	T °C	ρ (kg/m³)	μ (kg/ms)
Sky.P	30.00	1.16	1.87E-05
Bel 1.2.P	30.00	1.16	1.87E-05
Bel 2.2.P	19.10	1.20	1.82E-05

Fig. 11. The WT in DEFAM.

4.2 Experimental Methods

During the experiments, scaled-down models of Bel 1.2.V, Bel 2.2.V, and Sky.V were manufactured at a 1:40 scale and designated with the suffix P. As stated in the results, the Beluga buses (Bel 1.2 and Bel 2.2) exhibited the most significant reduction in drag, leading to the exclusion of the remaining four Beluga models from the experiment. To ensure accurate comparisons, the outcomes of the 1:40 experimental models are juxtaposed with the CFD solutions of the full-sized buses. The 1:40 scale domain has been assigned boundary conditions, including no-slip conditions for both the bus and road surfaces, at the outlet pressure is 1 atm and inlet velocities of 25.2, 28, and 35 m/s. To match the experiments, the road is assumed to be stationary. Table 1 lists the physical parameters utilized for the experimentation.

The WT experiments were conducted in Manisa Celal Bayar University, as shown in Fig. 11. The WT has a maximum velocity of 70 m/s, with a test section size of 300 mm x 300 mm and a test room length of 1000 mm. The overall length of the tunnel measures 6400 mm.

5. RESULTS

The computational results with actual dimensions are presented first, followed by a comparison of the

Table 2 First layer thickness, the Reynolds numbers and the drag coefficients at 27.7 m/s inlet velocity

Models	*y (m) first layer thickness*	Reynolds number	C_d
Sky.N	2.57E-05	2.65E+07	0.392
Sky.V	2.55E-05	2.48E+07	0.394
Bel.1.1.V	2.56E-05	2.56E+07	0.359
Bel.1.2.V	2.56E-05	2.53E+07	0.311
Bel.1.3.V	2.55E-05	2.51E+07	0.362
Bel.2.1.V	2.56E-05	2.61E+07	0.382
Bel.2.2.V	2.56E-05	2.55E+07	0.338
Bel.2.3.V	2.56E-05	2.53E+07	0.378

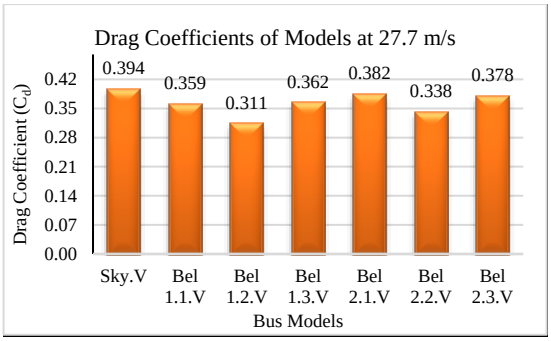

Fig. 12 Drag Coefficients of models at 27.7 m/s

experimental results with the computational results obtained from the reduced models.

5.1. The CFD Results

In this section, we present the computational fluid dynamics (CFD) results for both the Neoplan Skyliner and Beluga models. To validate the accuracy of the computations, the drag coefficient of the Sky.N model is initially calculated using the finite volume method. The manufacturer specifies a drag coefficient of 0.41, while our calculations yield a slightly lower value of 0.392, indicating good agreement between the CFD results and the provided information. In this section, a comprehensive comparison is conducted between the Beluga models and the Skyliner model, considering a volumetric space of 100 m^3 denoted by the suffix "V." Table 2 displays the details of the first cell at the wall, Reynolds numbers, and drag coefficients obtained from the analysis using the k-ω SST turbulence model. The simulations are conducted with an inlet fluid velocity of 27.7 m/s, and the y+ value is set to 1 for accurate predictions.

The slight reduction in size does not significantly impact the drag coefficients of the Beluga and Skyliner models. However, due to the change in cross-sectional area, the two Skyliner models are subjected to different drag forces. Specifically, the drag coefficient for Sky.N is measured at 0.392, while Sky.V exhibits a slightly higher value of 0.394. When comparing the drag coefficients of all Beluga models with that of the Sky.V model, which shares the same volume and area, it becomes evident that most of the Beluga models exhibit significant reductions in drag compared to the Sky.V model. Notably, Bel.1.2 exhibited the most significant drag reduction, followed by Bel.2.2. The drag coefficients of the buses outlined in Table 2 are visually contrasted in Fig. 12

Among the six beluga models, Bel.1.2 has the lowest drag coefficient of 0.311. In contrast, the Sky.V has the highest drag coefficient of 0.394 among the new designs. Figures 13 and 14 displays the static pressure distribution of the buses from side view and front view, respectively.

The front face of buses plays a crucial role in its aerodynamic performance, as it is the primary region where still air in the atmosphere first comes in contact. The effectiveness and impact of the front face on aerodynamics are significant, as it influences the generation of a stagnation point and the resultant pressure drag. Pressure drag is a force that resists the forward movement of the bus, and its magnitude increases with speed. To minimize drag and enhance efficiency, modifications to the front face design are necessary. By employing a curvier front face, it is possible to reduce the stagnation area and achieve smoother airflow. The interaction between the airflow and the side walls of a bus significantly impacts its aerodynamic performance. As the air shears of the front face and encounters the side wall, it flows over its surface. Initially, the airflow along the side wall is laminar, but as it progresses towards the rear, it transitions into a turbulent state, resulting in increased drag. The roof of the Beluga buses can be made similar to a flat model, with fluid flowing over it. This fluid flow is analyzed using the boundary layer theory. As the fluid moves beyond the center of the roof, a boundary layer forms, generating drag and creating a layer of turbulent airflow. Surface modifications are necessary to prevent these effects. The flow outside the boundary layer of the buses is affected by the contour of the boundary layer's edge, similar to how it would be influenced by the actual surface of an object. In certain instances, the boundary layer may separate or detach from the bus body, resulting in a modified effective shape that deviates from the physical shape of the buses. In order to tackle these challenges, modifications are made to the roof surfaces of the buses to mitigate the potential occurrence of boundary layer separation and turbulent flow. One strategy involves introducing an inclined surface on the roof, which aids in the separation of fluid flow and reduces the likelihood of boundary layer separation. This modification alters the flow pattern and plays a role in minimizing the detrimental effects caused by the boundary layer.

Bel.2.1.V has the highest static pressure at 528.92 Pa, while Bel.1.2 has the lowest at 450 Pa. The widest max. pressure area is in Sky.V, which lacks a perfect streamlined shape. In all Beluga models, the max. pressure areas are significantly reduced.

In the case of the bus, it is common to observe a negative pressure coefficient on specific areas like the top surface or the rear end. This negative pressure coefficient suggests that the pressure on those surfaces is lower than the atmospheric pressure. This creates a partial vacuum or suction effect, which can have beneficial effects. It can help generate downforce, which pushes the car down onto the road, increasing traction and improving stability. Additionally, it can aid in reducing drag, allowing the car

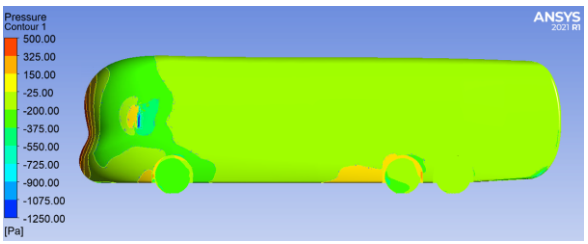

Bel 1.1.V

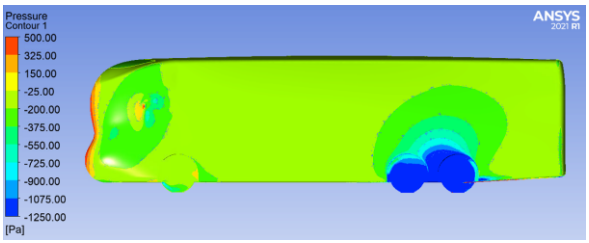

Bel 1.2.V

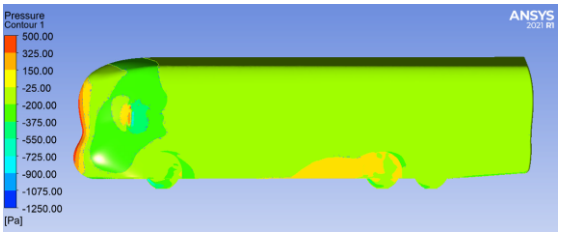

Bel 1.3.V

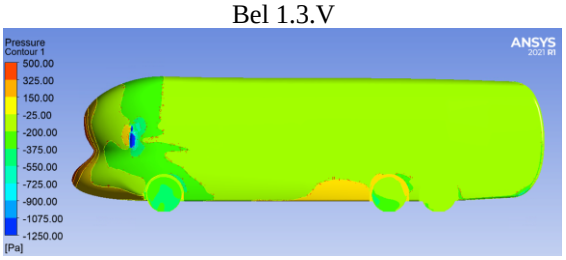

Bel 2.1.V

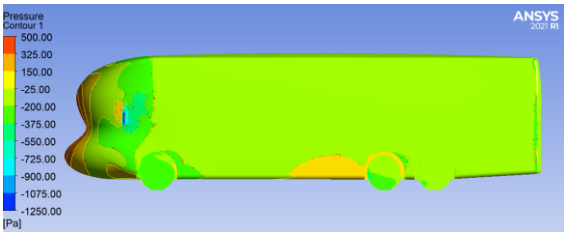

Bel. 2.2.V

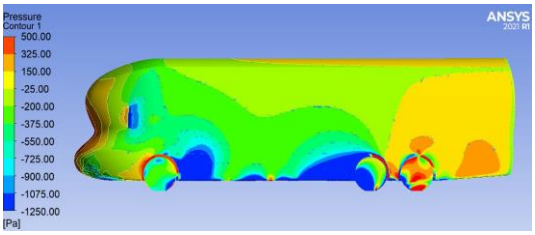

Bel 2.3.V

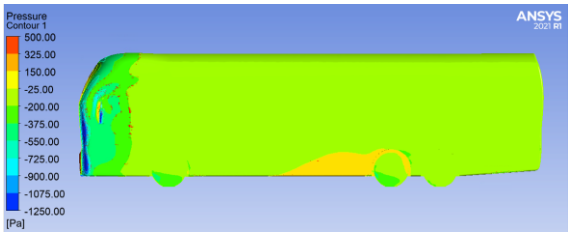

Sky.V

Fig. 13 Static pressure distribution from side view of bus models

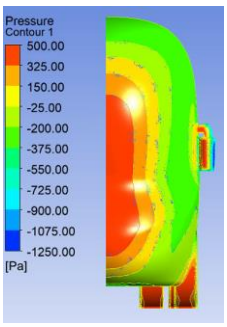

Bel 1.1.V

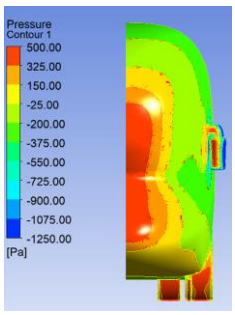

Bel 2.1.V

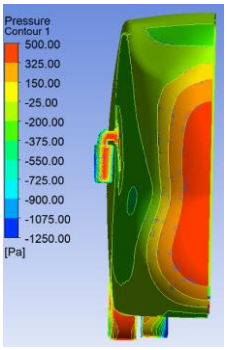

Bel 1.2.V

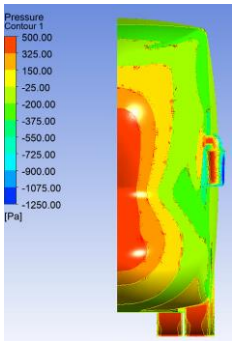

Bel 2.2.V

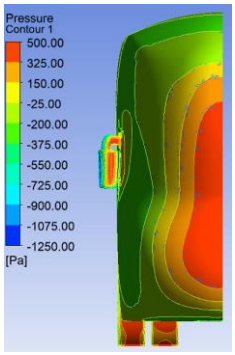

Bel 1.3.V

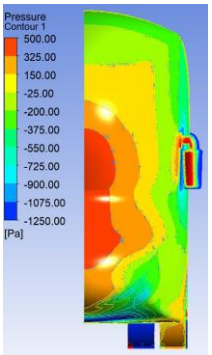

Bel 2.3

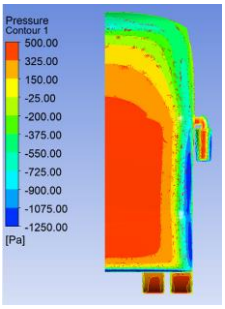

Sky.V

Fig. 14 Static pressure distribution from front view of bus models

to move through the air with less resistance, thereby enhancing overall performance. The graph pf pressure coefficient reveals that the front face area experiences a significant impact. This area creates a region where the air gets trapped momentarily, making it difficult for it to escape easily. The pressure coefficient (C_p) is measured at the bus and reported for the top part. We also probed the pressure acting on the body of the car in its symmetry plane with add points, and computed C_p for the top part.

The roof of the buses also contributes to a pressure coefficient of approximately -0.82 of Sky.V, -0.02 of Bel 1.2 (Fig.15), thereby increasing the drag force. By

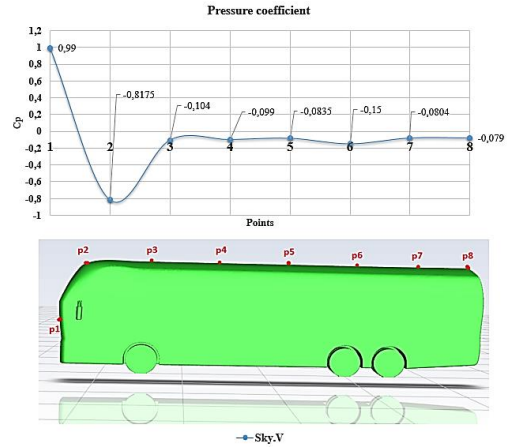

Sky.V

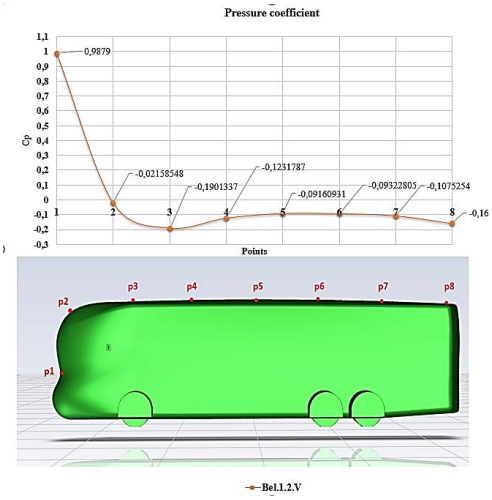

Bel 1.2.V

Fig. 15 Pressure coefficient graph of Sky.V and Bel 1.2.V bus models

examining the pressure coefficient graph, one can gain insight into the precise distribution of pressure coefficients over the bus body, providing a clear picture of the pressure coefficient scenario.

The presence of a nasal protrusion in whales, akin to the concept of a bow, serves to minimize the area affected by pressure. Similarly, the more curved front faces of Beluga buses contribute to the generation of a lower pressure coefficient area when compared to the Sky.V bus.

Figure 16 shows streamlines for the models, and eddies are shown at the rear of models.

Maintaining continuity of flow lines around a solid surface is aerodynamically beneficial, and this is exemplified by the performance of different bus models. Among them, the Bel 1.2 model stands out with its superior flow line continuity in the area, which results in less vortex behind the bus and a lower drag coefficient compared to other models. In contrast, the Skyliner V and x.3 models with equivalent rear body designs (Bel 1.3 V, Bel 2.3 V) exhibit significant vortex formation behind the bus, leading to higher wind resistance and reduced aerodynamic efficiency. In particular, the Skyliner V model has a noticeably high drag force compared to other

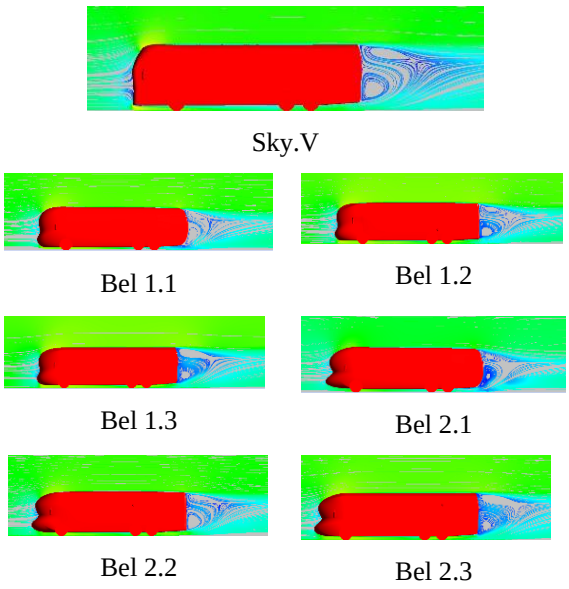

Fig. 16 Streamlines and eddies of the models

models, which is likely to increase fuel consumption. The flow of air around the bus was observed to compress at the front of the buses, leading to a high pressure as shown in Fig. 13 and 14. As the flow continued along the body of the bus, it moved smoothly until it reached the rear of the bus. At this point, the flow from different directions (top, bottom, and sides) converged and created a small vortex or recirculation of flow at the rear end of the body. The rounded shape of the bus helped to create a smoother flow of air in front of the bus, which reduced the impact of frontal pressure. Overall, the Bel 1.2 model has been demonstrated to have the best aerodynamic performance among the models considered. In buses, a significant part of the total drag force is due to pressure. The pressure-induced drag force is caused by the pressure distribution acting on the surface components of the body that are perpendicular to the flow. Flow vertically from the front surface of the bus is directed through the windscreen towards the top of the bus as shown in the streamline representation of the flow. The least pressure is seen at Bel 1.2. The new body designs have reduced the region of high pressure, resulting in improved aerodynamics. This approach has reduced the pressure-induced drag force in the front surface area of the bus where high pressure occurs.

5.2. The Experimental Results

Experimental studies used 1:40 scale prototypes of Skyliner, Bel.1.2, and Bel.2.1, named Sky.P, Bel.1.2.P, and Bel.2.2.P, respectively, as shown in Fig. 17. Only three models were compared, each with different head structures, including a Skyliner model (Sky.P), a Beluga head model (Bel 1.2 P), and a Beluga head with a 2.5 m extension intentionally left between the body and the head (Bel 2.2 P).

This section presents a repeated analysis, with both no-slip and non-moving road conditions used as the boundary conditions. The data presented in Table 3 was obtained using these boundary conditions.

Fig. 17 Experimental prototypes

Table 3 Experimental drag coefficients and CFD results data (for no-slip conditions-non-moving wall)

Models	V (m/s)	Re	C_d *(experimental)*	C_d *(CFD)*
Sky.P	25.2	5.65E+05	0.496	0.502
	28	6.27E+05	0.494	0.497
	35	7.84E+05	0.493	0.492
Bel. 1.2.P	25.2	5.75E+05	0.359	0.330
	28	6.39E+05	0.342	0.328
	35	7.99E+05	0.334	0.325
Bel. 2.2.P	25.2	5.80E+05	0.335	0.378
	28	6.45E+05	0.330	0.364
	35	8.06E+05	0.328	0.348

The results of WT tests, comprising the drag coefficients and Reynolds numbers for three inlet fluid velocities of 25.2, 28, and 35 m/s, are shown in Table 3.

The experimental results align well with the computational fluid dynamics (CFD) analysis indicating that the Bel.1.2 model exhibits the least drag coefficients at all flow velocities. The Bel.2.2 model outperforms the Skyliner model in all flow scenarios, exhibiting superior performance. To ensure a precise comparison of the computational data, a scaled-down version of 1:40 is employed for the computational fluid dynamics (CFD) analysis. The obtained results are then appropriately compared and evaluated. Figure 18 provides a comparison of drag coefficients for the Sky.P model. The discrepancy at low Reynolds numbers between the experimental and numerical simulations may stem from a variety of factors, including the assumptions made during the simulation, the boundary conditions, and the precision of the measurements taken during the experiment. While the utilization of RANS-type turbulence models in CFD analysis poses certain challenges, it offers significant advantages compared to WT experiments. CFD analysis allows for a comprehensive and detailed examination of the spatial distribution of wind velocity, surpassing the limited information obtained through WT testing. Notably, the CFD simulation can successfully identify wind points that might have been overlooked in tunnel experiments. Additionally, WT experiments inherently entail uncertainties, such as measurement instrument errors, and inaccuracies in sensor placement. Conversely, CFD eliminates such uncertainties. Another significant advantage lies in the ability to simulate arbitrary approach flows in CFD, a freedom not easily attainable in WT testing. Consequently, it becomes feasible to minimize the disparity in estimation accuracy between WT experiments and CFD in practical assessments. It is known that viscous effects are more pronounced at low Reynolds numbers. These effects can cause a more complex distribution of the flow and change the drag coefficient. Therefore, it can be thought that the differences between the experimental and analytical results may be due to viscous effects. At low Reynolds numbers, the viscous forces tend to smooth out the flow, causing it to adhere closely to the object's surface and resulting in a higher drag coefficient compared to the idealized, inviscid flow assumption.

Figures 19 and 20 present a comparison of drag coefficients for the Bel.1.2 and Bel.2.2 models against Reynolds numbers. As the Reynolds number increases, the disparities among the outcomes diminish.

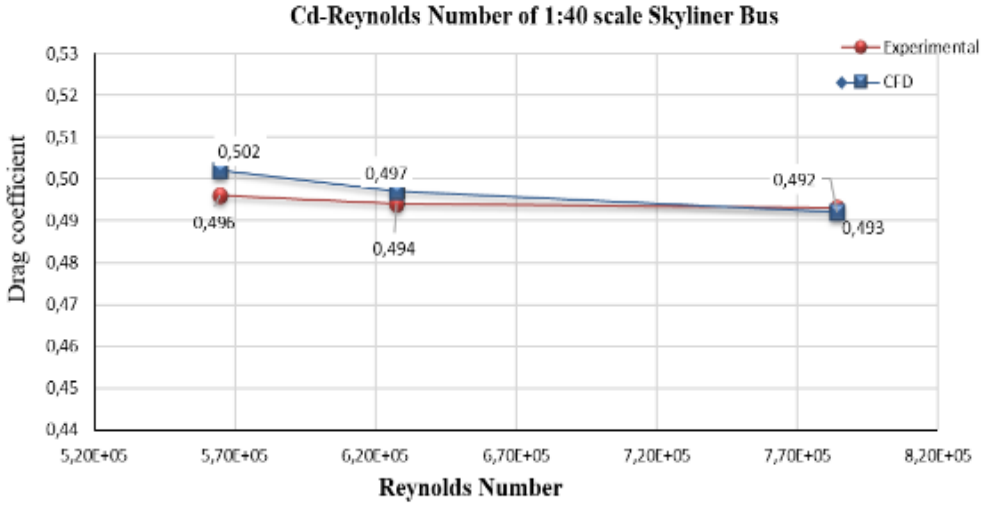

Fig. 18 Drag coefficients of Sky.P

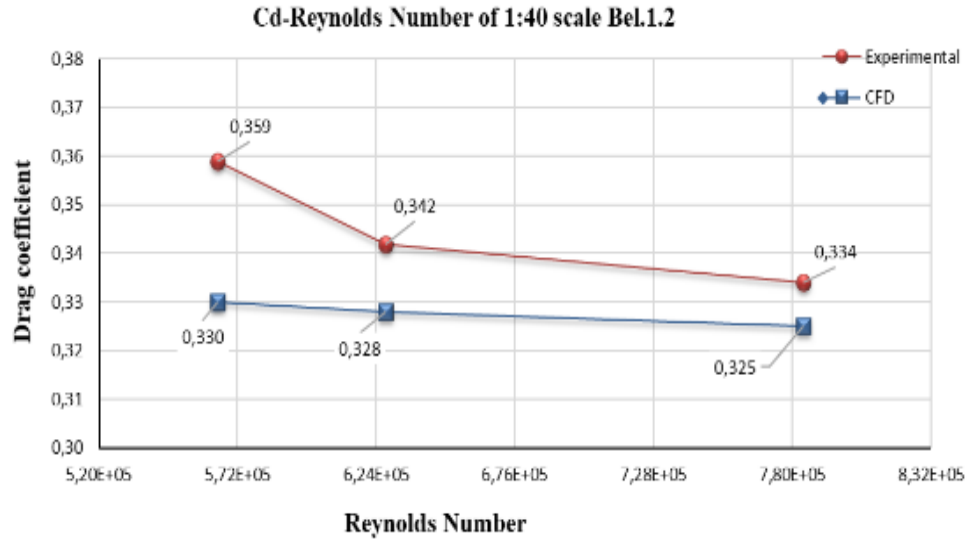

Fig. 19 Drag coefficients of Bel 1.2.P

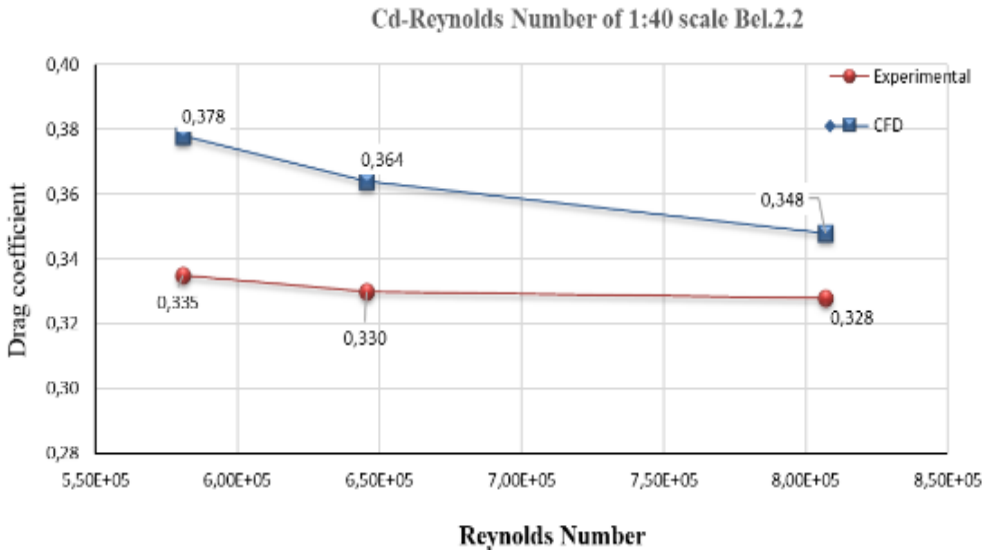

Fig. 20 Drag coefficients of Bel 2.2.P

Overall, there is reasonable agreement between the experimental and computational results, with both indicating that the new nature-inspired designs have lower drag coefficients and forces compared to the existing design.

6. CONCLUSION

The objective of this study is to improve the aerodynamic efficiency of buses by integrating design elements inspired by beluga whales. Six distinct variations of bus designs inspired by the beluga whale are assessed and compared to the Skyliner model, which already demonstrates one of the most minimal drag coefficients currently available. The findings reveal that significant reductions in drag coefficients are possible by emulating the shape of a beluga whale, with coefficients as low as 0.311, in contrast to conventional designs with coefficients as high as 0.394.

The drag coefficients of all six models of the bus designs inspired by beluga whales exhibited a noticeable reduction with the most significant improvement seen in the Bel.1.2 model, which achieved a 21.06% reduction. Using the average reduction in drag coefficient, it is estimated that the new beluga design will result in a fuel consumption reduction of approximately 12.64%, which is around 0.6 times the drag coefficient reduction (Fred, 2005). Despite some minor numerical differences between the results, which are within an acceptable deviation of a few percent, the study concludes that the shapes and structures found in nature can provide valuable inspiration for improving bus aerodynamics. Achieving fuel savings through such improvements will reduce carbon dioxide release to the atmosphere, maintaining a sustainable future.

ACKNOWLEDGEMENTS

Manisa Celal Bayar University's support is highly esteemed.

Availability of data and materials

The authors can provide the experimental and numerical data upon request.

Funding Information

This project is carried out at Manisa Celal Bayar University with the projects numbered BAP 2012-020 and BAP 2013-037.

Authors Contributions

Seda Kırmacı Arabacı has completed her Ph.D. thesis under the supervision of Prof. Mehmet Pakdemirli. As part of her research, Arabacı carried out WT experiments and numerical simulations using FLUENT. Pakdemirli provided the research topic and supervised the entire process, including manuscript writing, result checking, and interpretation.

REFERENCES

Ahmad, N. E., Aboserie, E., & Gaylard, A. (2010). Mesh optimization for ground vehicle Aerodynamics, *CFD Letters*, 2(1), 54–65.

Alamaan, A., Ashraf, A. O., & Waqar, A. (2014). Passive drag reduction of square back road vehicles. *Journal of Wind Engineering and Industrial Aerodynamics*, 134, 30-43. https://doi.org/10.1016/j.jweia.2014.08.006

Belzile, M., Patten, J., McAuliffe, B., Mayda, W., & Tanguay, B. (2012). Technical report: review of aerodynamic drag reduction devices for heavy trucks and buses. *Project*, 54-A3578

Benyus, J. M. (2002). *Biomimicry: Innovation inspired by nature perennial*. New York.

Bhave, A., & Taherian, H. (2014). *Aerodynamics of intercity bus and its impact on co_2 reductions*. Proceedings of the 14th Annual Early Career Technical Conf. The University of Alabama Birmingham, USA, 165-172.

Daimler, A. G., & Mercedes-Benz (2011). *Consept vehicles and visions Evolution of Innovations 96-97*. https://www.daimler.com/documents/innovation/other/daimler-theresearchcarsofmercedesbenz-en-2011.pdf)

Ferziger, J. H., Peric, M., & Street R. L. (2019). *Computational methods for fluid dynamics*. Springer Verlag.

Fish, F. E., Weber, P. W., Murray, M. M., & Howle, L. E. (2011). The tubercles on humpback whales' flippers: Application of bio-inspired technology. *Integrative and Comparative Biology*, 51(1), 203–213. https://doi.org/10.1093/icb/icr016

Fluent, ANSYS, (2012). *Ansys Fluent 14.5 User's Guide*. ANSYS, Inc., Canonsburg, PA.

Fred, B. (2005). Reducing Aerodynamic Drag and Fuel Consumption Global Climate and Energy Project Workshop on Advanced Transportation Stanford University, ABD 5.

Håkansson, C. & Lenngren, M .J. (2010). *CFD analysis of aerodynamic trailer devices for drag reduction of heavy duty trucks.* Master's Thesis, Automotive Engineering Chalmers University of Technology Göteborg Sweden . http://www.airbus.com/aircraftfamilies/freighter/beluga (Access date: 16.04.2015)

Hu, X., & Wong, T. (2011). A numerical study on rear-spoiler of passenger vehicle. *World Academy of Science Engineering and Technology*, 81 636–641.

Jasak, H. (1996). *Error analysis and estimation for finite volume method with applications to fluid flow* [PhD thesis, Department of Mechanical Engineering]. Imperial College of Science, Technology and Medicine, London.

Jones, W. P., & Launder, B. E. (1973). The prediction of laminarization with a two-equation model of turbulence, international journal of heat and mass transfer. *Physics Engineering*, 14, 119-132. https://doi.org/10.1016/0017-9310(72)90076-2.

Launder, B. E., & Spalding, D. B. (1974). The numerical computation of turbulent flows. *Computer Methods in Applied Mechanics and Engineering* 3(2), 269–289. https://doi.org/10.1016/0045-7825(74)90029-2.

Mohamed, E. A., Radhwi, M. N., & Abdel Gawad, A. F. (2015). Computational investigation of aerodynamic characteristics and drag reduction of a bus model *American Journal of Aerospace Engineering*, 2(1), 64-73. https://doi.org/10.11648/j.ajae.s.20150201.16

Nowak, R. M. (1991). *Walker's mammals of the world 2*. (5 ed.) Baltimore: The Johns Hopkins University Press ISBN 0-8018-5789-9.

Patil, C. N., Shashishekar, K. S., Balasubramanian, A. K., & Subbaramaiah, S. V. (2012). Aerodynamic study and drag coefficient optimization of passenger vehicle. *International Journal of Engineering* Research & Technology, 1(7). https://doi.org/10.17577/IJERTV1IS7079

Roy, S., & Srinivasan, P. (2000). External flow analysis of a truck for drag reduction *International Truck and Bus Meeting & Exposition*, 01(2000)3500.

Singha, S., Zunaid, M., Ansari, N. A., Bahirani, S., Dhall, S., & Kumar, S. (2014). Numerical study of the generic sports utility vehicle design with a drag reduction Add-On device. *Journal of Computational Engineering*, ID:785294, 1-17.

Sudin, M. Z., Abdullah, M. A., Shamsuddin, S. A., Ramli, F. R., & Tahir, M. M., (2014) Review of research on vehicles drag reduction methods. *Int Journal of Mechanical & Mechatronics Engineering*, 14(2), 35-47.

Trinh, M. H., Do, T. Q., & Nguyen, T. H. (2022). Study on the dynamic instability of a bus in crosswind

conditions. *Engineering and Technology for Sustainable Development*, 32(1) 43-51. https://doi.org/10.51316/jst.156.etsd.2022.32.1.7

Wilcox, D. C. (1988). Reassessment of the scale-determining equation for advanced turbulence models, AIAA Journal 26 (11), 1299– 1310. https://doi.org/10.2514/3.10041.

Wilcox, D. C. (2006). *Turbulence modeling for CFD*. DC W Industries.

Wilcox, D. C. (2008). Formulation of the k-ω turbulence model revisited, AIAA Journal 46 (11), 2823–2838. https://doi.org/10.2514/1.36541.

Wood, R. (2015). Reynolds number impact on commercial vehicle aerodynamics and performance, *SAE International Journal of Commercial Vehicles*, 8(2), 590-667. https://doi.org/10.4271/2015-01-2859.

Yan, Y. Y. (2007). Recent advances in computational simulation of macro, meso and micro-scale biomimetics related fluid flow problems. *Journal of Bionic Engineering*, 4(2), 97–107. https://doi.org/10.1016/S1672-6529(07)60021-3

Yudianto, A., Sofyan, H., & Fauzi, N. A. (2022). Aerodynamic characteristics of overtaking bus under crosswind: CFD investigation. *CFD Letters*, 14(8), 20-32. https://doi.org/10.37934/cfdl.14.8.2032